ACS OMEGA

Article

To Enhance the Performance of $LiNi_{0.5}Co_{0.2}Mn_{0.3}O_2$ Aqueous Electrodes by the Coating Process

Wenchang Jiang, Yilan Jiang, and Chun Huang*

Cite This: *ACS Omega* 2024, 9, 21006−21015

Read Online

ACCESS | Metrics & More | Article Recommendations | Supporting Information

ABSTRACT: The Li^+/H^+ cation exchange reactions occur when the cathode is exposed to water and can cause the degradation of battery performance, posing a significant challenge in the preparation of cathode aqueous electrodes. In this study, kh570 [3-(trimethoxysilyl)propyl methacrylate] is used to coat and modify the surface of $LiNi_{0.5}Co_{0.2}Mn_{0.3}O_2$ cathode particles. During the coating process, kh570 undergoes hydrolysis to generate silanol groups, which are subsequently bonded onto the surface of cathode particles and undergo self-polymerization through condensation reactions. As a result, a coating layer forms on the surface of the cathode. This change alters the surface properties of the cathode particles from hydrophilic to hydrophobic, thereby increasing their resistance to water. The coating layers reduce direct contact with water and minimizes internal particle microcracks formation in aqueous electrode processing. After the preparation of aqueous electrodes, the modified cathode exhibits lower transfer resistance and lower polarization, improving both the current rate performance and the cycling performance of the battery.

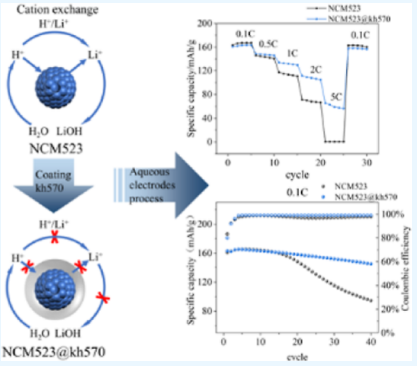

1. INTRODUCTION

Since their commercialization by Sony in 1991, lithium-ion batteries have played an important role in the field of energy storage due to their high energy density (200−500 W h kg^{-1}).[1] Advancements in manufacturing technology have significantly reduced the costs of lithium-ion batteries, driving the development and prosperity of electric vehicles (EVs). As a result, the global market size for lithium-ion batteries has rapidly expanded to USD 48.19 billion in 2022 and is projected to reach USD 182.53 billion by 2030.[2] However, there are still numerous challenges in reducing costs and achieving vehicle electrification goals. Therefore, technological innovation is necessary to develop low-cost, high-energy, and high-power Li-ion batteries.

The electrode process is the initial and critical step in manufacturing lithium-ion batteries. It involves three main processes: slurry preparation, coating, and the subsequent drying process. The selection of polymer binders and solvents not only plays a critical role in preparing stable slurry but also significantly impacts performance and cost of batteries. Currently, poly(vinylidene fluoride) (PVDF) binder is widely employed in the industrial sector for cathode electrodes. This is due to its excellent electrochemical stability at the potential range of 0−5 V (vs Li/Li^+),[3] suitable cohesion between active materials and current collector, as well as appropriate rheology for the coating process rheology for coating process.[4] The organic solvent *N*-methyl-2-pyrrolidone (NMP) is commonly employed to dissolve PVDF in industrial manufacturing. However, NMP is costly and has reproductive toxicity,[5] which increases manufacturing costs and poses potential hazards to the physical health of workers. Therefore, developing low-cost, environmentally friendly solvents and binders is necessary to meet future development requirements. The combination of aqueous solvent with water-soluble binders is the most ideal strategy, which has been successfully applied in the industrial-scale production of graphite anode electrodes (CMC and SBR as a composite binder).[6] However, the commercial success of the cathode aqueous electrode still faces numerous challenges. The selection of water-solution binders is important work to improve the performance of cathode aqueous electrodes. Kuenzel et al. utilized guar gum as a binder for $LiNi_{0.5}Mn_{1.5}O_4$ cathode electrodes to improve cycling stabilities, further cross-linking with CMC through citric acid can improve current rate capability.[7] Sun et al. utilized carboxymethyl chitosan as a binder for $LiFePO_4$ cathode electrodes and demonstrated that it exhibited comparable cycling capability to PVDF at high rates.[8] Utilizing xanthan gum as a binder for Li-rich layered oxide cathode electrodes can effectively suppress voltage decay and achieve excellent cycling stability at both room and elevated temperatures.[9] Loeffler et al. found that polyurethane binder can encapsulate $LiNi_{1/3}Mn_{1/3}Co_{1/3}O_2$ during the slurry and coating

Received: January 9, 2024
Revised: March 30, 2024
Accepted: April 15, 2024
Published: April 29, 2024

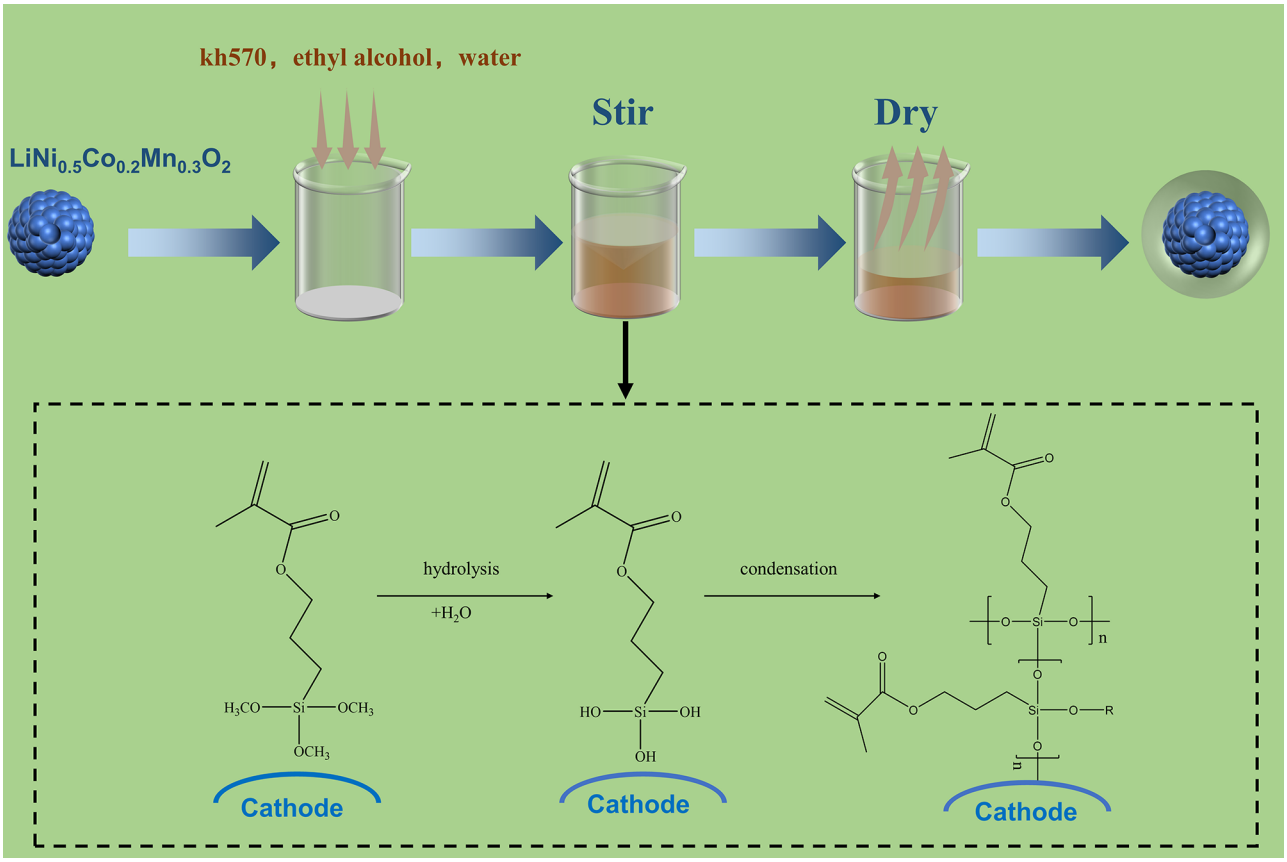

Figure 1. Coating process and reaction mechanism.

process resulting in greatly decreasing the corrosion of the aluminum foil current collector.[10] Other types of water-soluble polymers, such as chitosan,[11] LiPAA,[12] CMC,[13] and so on, have also been attempted to be utilized as binders for aqueous cathode electrodes. Furthermore, some companies are involved in the design and synthesis of innovative binders. Blue Ocean & Black Stone in Beijing and Indigo in Chengdu are representative companies and have currently become industry leaders.[14] Some research reports that the LA132 and LA133 binders, synthesized by Indigo Company, can improve the cycle life of cathode electrodes due to their strong adhesion performance resulting from the high polarity of acrylonitrile.[15] In this study, we utilized LA132, a triblock copolymer consisting of acrylamide (AM), lithium methacrylate (LiMAA), and acrylonitrile (AN), as the binder to prepare aqueous electrodes.

Although many water-soluble polymers have been utilized in preparing cathode electrodes so far. There are still intricate challenges to substitute NMP with water due to the occurrence of Li^+/H^+ cation exchange reactions when cathode materials are exposed to water.[16,17] The Li^+/H^+ cation exchange reactions are particularly serious for high-energy density $LiNi_xCo_yMn(Al)_{1-x-y}O_2$ cathode materials, which are widely applied in the commercial: The Li^+ ions migrate from the lattice outward to the surface where they then react with CO_2 and H_2O to form lithium hydroxide, bicarbonates, and carbonates. Simultaneously, H^+ migrates in the opposite direction and attaches to the corner oxygen atom in one of the CoO_6 octahedra. Equations 1−3 describes the chemical process.

$$Li^+ + H_2O \rightarrow H^+ + LiOH \quad (1)$$

$$LiOH + CO_2 \rightarrow LiHCO_3 \quad (2)$$

$$LiOH + LiHCO_3 \rightarrow H_2O + Li_2CO_3 \quad (3)$$

Additionally, Ni^{3+} reduces to Ni^{2+} and forms rock salt phase NiO at the cathode surface.[18] The pH of the $LiNi_xCo_yMn(Al)_{1-x-y}O_2$ cathode aqueous slurry usually was strong alkalinity due to the high concentration of LiOH. It can corrode the aluminum current collector and increase resistance. As the aluminum foil corrodes the reaction anyway, H_2 is generated at the same time.[19,20] The integrity of the cathode electrodes may be damaged due to the generation of cracks when H_2 bubbles are emitted during the coating process.[21] The above reactions degrade the capacity and cycle life and increase the polarization of the cathode electrodes.[16,22]

To mitigate the Li^+/H^+ cation exchange reaction, several researchers propose diverse strategies. The application of the cathode particles coating to enhance resistance to water is one of the methods. Tanabe et al. utilized carbon, AlO_x, NbO_x to coat $LiNi_{0.5}Mn_{1.5}O_4$ and suppressed the degradation of the cycle caused by contacting water with the cathode surface.[23] They also researched the TiO_x coating layer on the $LiNi_aCo_bAl_{1-a-b}O_2$ surface. The coating layers improve the specific capacity of aqueous cathode electrodes.[24] Hofmann et al. utilized Li_3PO_4 as a coating layer for $LiNi_xCo_yAl_{1-x-y}O_2$ to suppress Li^+ leaching and decreased the alkalinity of the cathode slurry, thereby optimizing battery performance.[25] Watanabe et al. used H_3PO_4 to form a Li_3PO_4 coating layer on the $LiNi_xCo_yAl_{1-x-y}O_2$ ($x > 0.85$) surface, thereby enhancing cyclability and high-rate performance.[26]

https://doi.org/10.1021/acsomega.4c00301
ACS Omega 2024, 9, 21006−21015

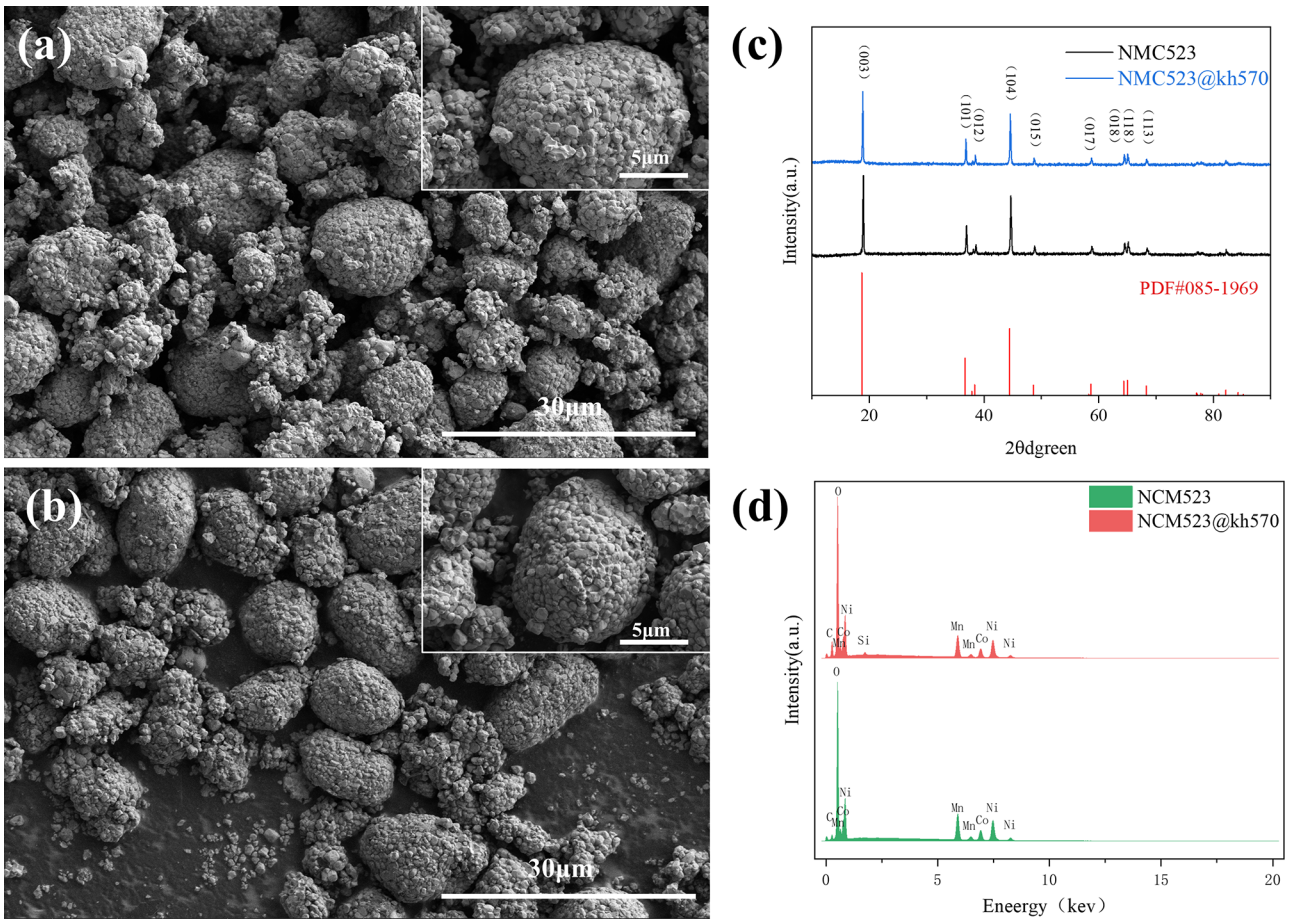

Figure 2. SEM images of (a) pristine NCM523 particles and (b) NCM523@kh570 particles; (c) XRD patterns of NCM523 and NCM523@kh570 particles; (d) EDS spectra of NCM523 and NCM523@kh570 particles.

Although current inorganic coating schemes can enhance resistance to water and improve the electrochemical performance of cathode aqueous electrodes, their implementation requires sintering at 300 to 600 °C, resulting in increased energy consumption and material preparation costs. Simultaneously, the performance of cathode aqueous electrodes prepared by the existing schemes still falls short of meeting the requirements for industrial-scale production. In this work, we proposed an organic hydrophobic coating layer strategy to modify the surface of $LiNi_{0.5}Co_{0.2}Mn_{0.3}O_2$ particles, which can be implemented at a low temperature (<100 °C) and improve the performance of cathode aqueous electrodes. We chose kh570 (3-(trimethoxysilyl)propyl methacrylate) as a coating reagent which is usually utilized for the modification of solid surfaces.[27] Figure 1 shows the coating mechanism and process: after contact with small doses of water, kh570 undergoes a hydrolysis reaction to form silanol groups. The silanol groups undergo a polycondensation reaction and also bond with the hydroxyl on the surface of the solid and then form polymeric coating layers on the surface of the solid. Due to the abundance of ester functional groups in the coating layers, the solid surface transforms form hydrophilic into hydrophobic. The coating layers can protect cathode particles by reducing direct contact with water during the cathode aqueous electrode process.

2. EXPERIMENTAL SECTION

2.1. Materials. The kh570 (98%, RG) was obtained from the Admas company. The ethanol (97%, AR) was obtained from the Greagen company. The $LiNi_{0.5}Co_{0.2}Mn_{0.3}O_2$ particles (NCM523) were produced by Beijing Easpring company. The LA132 (15% solid content) was produced by Indigo company.

2.2. Cathode Coating. 0.36 g of kh570, 4 g of ethanol, 18 g of NCM523, and 0.36 g of deionized water were added to a 25 mL beaker and magnetically stirred for 4 h at room temperature. Subsequently, the mixture was dried at 60 °C for 3 h and 80 °C overnight to obtain modified particles NCM523@kh570.

2.3. Electrodes Preparation. 3.6 g of LA132 (3.6 g) was diluted in water (4.5 g) by magnetically stirring for 30 min in a 25 mL beaker. Subsequently, 0.27 g of SP (conductive black) was added and magnetically stirred for 1 h. Then, 12.69 g of NCM523 particles were added and magnetically stirred for 1.5 h to obtain a slurry. The slurry was coated on a 16 μm aluminum foil using a doctor blade coater and subsequently dried at 60 °C for 3 h and 80 °C overnight. The dried electrodes were punched into pieces with a diameter of 1.5 cm to obtain NCM523 electrodes. The same process was employed to prepare the NCM523@kh570 electrodes.

2.4. Batteries Assembly and Measurement. The cathode electrods with a mass loading of 8-9 mg cm^{-2}were selected to assemble CR2032 type coin cells in an Ar-filled glovebox atmosphere (H_2O < 0.1 ppm, O_2 < 0.1 ppm). Lithium metal foils with a diameter of 16 mm were used as

https://doi.org/10.1021/acsomega.4c00301
ACS Omega 2024, 9, 21006−21015

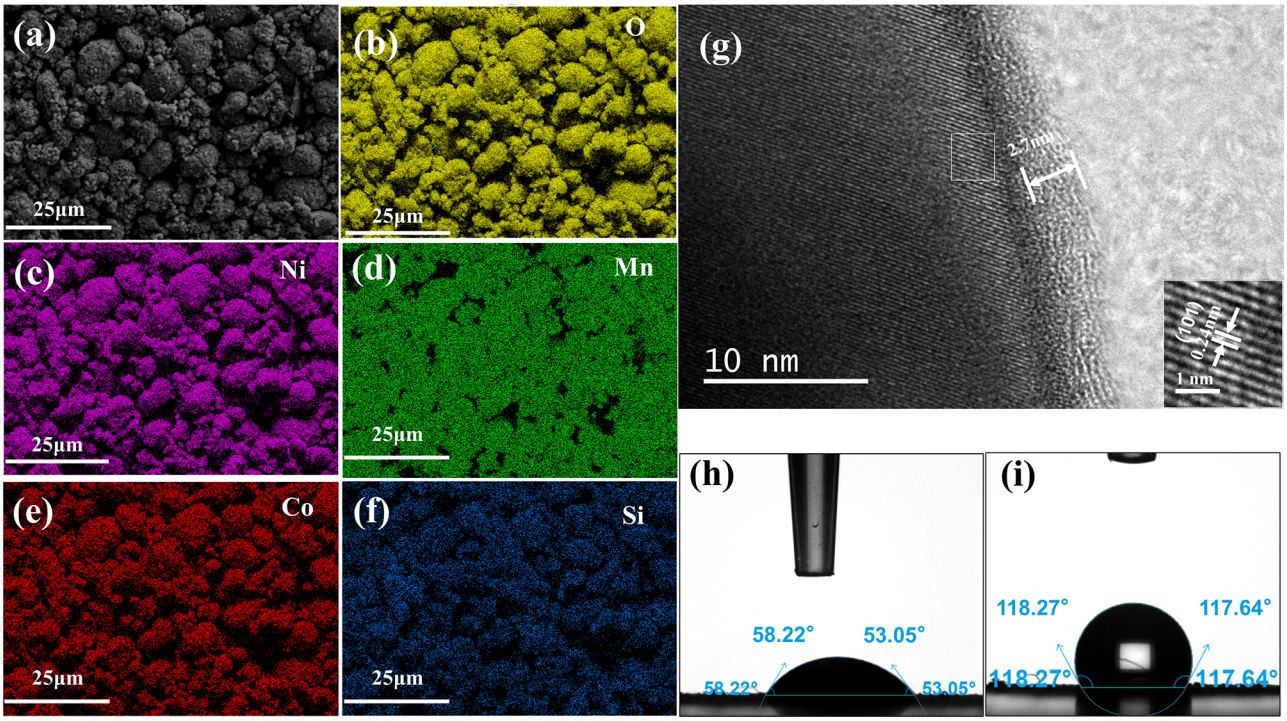

Figure 3. (a) SEM images of NCM523@kh570 and the corresponding EDS mapping of (b) O, (c) Ni, (d) Mn, (e) Co, and (f) Si; (g) HRTEM images of NCM523@kh570; Contact angles of (h) NCM523 and (i) NCM523@kh570 with water.

anode. The polypropylene film (Celgard 2500) with a diameter of 19 mm was used as the separator. Each cell was filled with 180 μL of electrolyte with 1 mol L^{-1} $LiPF_6$ dissolved in a mixture of ethylene carbonate (EC) and dimethyl carbonate (DMC) at a volume ratio of 1:1. Cyclic voltammetry (CV) was tested by electrochemical workstations (Gamry interface 5000E) with a potential range of 2.8−4.3 V (vs Li/Li^+) and a scan rate of 0.1 mV s^{-1}. Electrochemical impedance measurements were conducted by an electrochemical workstation (Gamry interface 5000E) at frequencies ranging from 0.1 to 10^5 Hz with a potential perturbation of 5 mV. The capacity and cycling performance were tested by LAND CT2001A at the potential range of 2.8−4.3 V (vs Li/Li^+), with a rest time of 5 min between charge and discharge process. All electrochemical measurements are conducted at 25 ± 0.5 °C.

2.5. Characterization. The cross sections of the electrodes were prepared by an argon ion polishing system (Ilion II 697, Gantan company). The morphologies and element mapping images of cathode particles were characterized by an Apreo (Thermo Fisher company) field emission scanning electron microscope. The morphologies of electrodes were characterized by a JEM-7800F field (Jeol company) emission scanning electron microscope. The connect angles were measured by Optical Tensiometer (Theta Flex, Biolin company). The crystal structures were characterized by XRD (Bruker AXS D8 ADVANCE) using Cu-Kα radiation ($10° < 2\theta < 90°$). Diffraction patterns were recorded at a scanning angle of 2° min^{-1} and a step size of 0.02°. The coating layers and crystal lattice on the surface were characterized by HRTEM (Tecnai G2 F20, FEI company) at acceleration voltage of 200 kV. The pH value was measured by pH meter (PHS-3C, Shanghai INESA Scientific company). The resistance of electrodes was measured using a multifunctional resistance testing instrument (BER2500, IEST company).

3. RESULTS AND DISCUSSION

The morphologies of NCM523 and NCM523@kh570 are shown in Figure 2a,b, respectively. Both pristine and modified particles exhibit distinct polycrystalline morphologies, with the majority of the particles displaying a spherical polycrystalline morphology and a minority exhibiting an irregular polycrystalline morphology. The average diameter of pristine and modified particles is approximately 10 μm, which consists of primary particles with an approximate size of about 500 nm. The morphology of the NCM523 particles and NCM523@kh570 particles is highly similar, suggesting that the cathode particles remain intact during the coating process.

The crystal structures were characterized by XRD and the diffraction pattern is shown in Figure 2c. Both the diffraction peaks of NCM523 and NCM523@kh570 particles show a typical hexagonal α-$NaFeO_2$ structure, belonging to $R\bar{3}m$ space group (JCPDF card no. 85-1969).[28] The crystalline structures of the two kinds of particles are nearly identical, indicating that the chemical reactions initiated by kh570 in the coating process do not disrupt the crystal structure of Li-$Ni_{0.5}Co_{0.2}Mn_{0.3}O_2$. The results also demonstrate that no new crystalline material is introduced during the coating process. The EDS spectrum is shown in Figure 2d. Comparing the NCM523 spectrum, a new peak of Si is observed in the NCM523@kh570 spectrum, suggesting that kh570 has been bonded to the cathode particles.

To investigate the uniformity of the coating layers in the particles, we employed EDS to characterize the elemental mapping of NCM523@kh570. The SEM image of NCM523@kh570 is shown in Figure 3a, and the associated elemental mapping images of O, Ni, Mn, Co, and Si are shown in Figure 3b−f, respectively. The elemental distribution of O, Ni, Co, and Mn follows the distribution of particles since they are intrinsic elements. Figure 3f demonstrates that Si, which is a

https://doi.org/10.1021/acsomega.4c00301
ACS Omega 2024, 9, 21006−21015

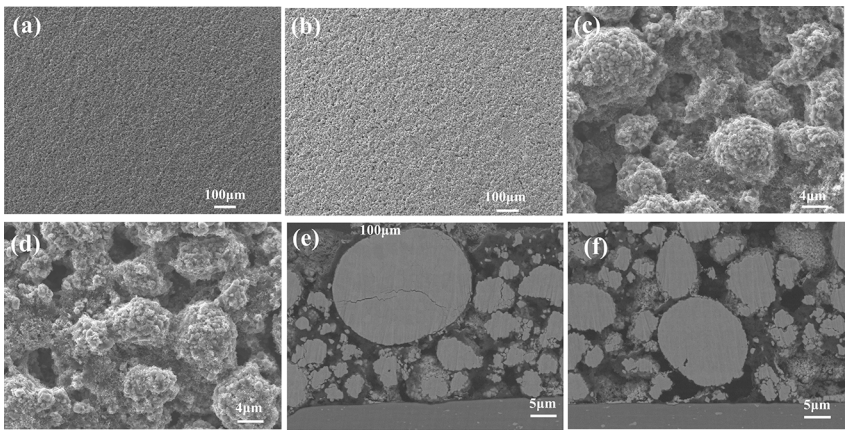

Figure 4. Top images at 100× of (a) NCM523 electrodes and (b) NCM523@kh570 electrodes; at 3000× of (c) NCM523 electrodes and (d) NCM523@kh570 electrodes; and the cross-sectional images of (e) NCM523 electrodes and (f) NCM523@kh570 electrodes.

characteristic element of kh570, exhibits same distribution mapping as other elements. This indicates that kh570 has been effectively and uniformly bonded to the surface of cathode particles. To further investigate the thickness and structure of the coating layers, the NCM523@kh570 particles were dispersed in deionized water for 5 min and adhered to copper mesh. Subsequently, the NCM523@kh570 particles were characterized by HRTEM. In Figure 3g, HRTEM images of NCM523@kh570 particles show the presence of an amorphous layer with a thickness of 3−4 nm on the surface. It can be inferred that the amorphous layer is an organic coating layer formed by the polymerization of kh570. Furthermore, there are also obvious lattice streaks in the HRTEM image with a lattice spacing of 0.24 nm, which corresponds the (101) interplanar crystal spacing of $LiNi_{0.5}Co_{0.2}Mn_{0.3}O_2$ ($R\bar{3}m$).[29] It also illustrates that the crystal structure of the cathode particles remains intact after the coating process.

To investigate the impact of the coating layers on the surface properties of cathode particles, we measured the contact angles of the NCM523 and NCM523@kh570 powders with water. The powders were coated on double-faced adhesive tape with another side adhesive on a glass sheet. Subsequently, the sample was compacted by using another glass sheet. The resulting sample is shown in Figure S1. The contact angles of pristine NCM523 and NCM523@kh570 powders with water are shown in Figure 3h,i, respectively. The contact angle of NCM523 ranges from 53.05 to 58.22°, indicating its hydrophilic nature. However, coating NCM523 with kh570 significantly increases the contact angle to a range of 117.64−118.27°, suggesting a transformation to hydrophobicity on the surface of particles. The alteration of the surface property of cathode particles is attributed to the presence of a substantial number of hydrophobic ester bonds in the coating layers. The pH values of NCM523 and NCM523@kh570 slurry are 11.03 and 10.85, respectively. This indicates that the hydrophobicity layers reduce direct contact between the cathode particles and water, thereby mitigating the Li^+/H^+ cation exchange reactions during aqueous electrodes processing.

The top and cross-sectional morphologies of NCM523 and NCM523@kh570 aqueous electrodes were investigated by SEM. The top microscopic morphology of NCM523 and NCM523@kh570 electrodes at 100× is presented in Figure 4a,b, respectively. Both two types of electrodes exhibit a uniform, crack-free, and flat topography. The top microscopic morphology of NCM523 and NCM523@kh570 electrodes at 3000× is presented in Figure 4c,d, respectively. Both two types of electrodes exhibit a uniform distribution of binders, particles, and conductive additives topography, which plays a critical role in performance of batteries.[30] The results demonstrate that the alteration of the surface characteristics of cathode particles has not had an adverse effect on the dispersion of particles in the slurry process. The cross-sectional morphology of NCM523 and NCM523@kh570 electrodes is shown in Figure 4e,f, respectively. In Figure 4e, certain microcracks can be observed along the intergranular boundaries within spherical polycrystalline particles in the NCM523 electrodes. In Figure 4f, no visible microcracks are observed in the NCM523@kh570 electrodes. The results are consistent with previous reports that the intergranular bonding of polycrystalline $LiNi_xCo_yMn_{1-x-y}O_2$ becomes fragile when exposed to water and the agitation process.[31] The formation of new microcracks leads to the creation of additional surfaces, which enhances the extent of interaction with water and facilitates the reconstruction of the interfacial structure, resulting in the formation of a new NiO layer.[16,32,33] The results demonstrate the effectiveness of the hydrophobic coating layers in protecting cathode particles during aqueous electrodes processing.

The multifunctional resistance testing instrument is shown in Figure S2. Figure 5 shows the specific resistance of electrodes under different levels of pressure intensity. The specific resistances of NCM523 electrodes at 5, 15, 30, 45, and 60 MPa are 24,088, 9572, 2900, 1295, and 736 Ω·cm, respectively. For NCM523@kh570 electrodes, the specific resistances are as follows: 10,451, 3635, 1157, 562, and 333 Ω·cm, respectively. The specific resistance of NCM523@kh570 electrodes is obviously lower than that of NCM523 electrodes. In aqueous slurry, the cation exchange reaction of Li^+/H^+ between cathode particles and water can generate LiOH and achieve chemical equilibrium in a short time.[20] When coated on the aluminum foil current collector, the alkaline slurry can corrode the foil and disrupt the chemical equilibrium, further promoting the cation exchange reaction of Li^+/H^+ reactions. The hydrophobic coating layers effectively surppress this process, thereby reducing corrosion between the aqueous slurry and the aluminum foil current collector. As a result, specific resistance of electrodes is reduced.

The electrochemical performance of the batteries are assessed in Figure 6, with the NCM523 and NCM523@

https://doi.org/10.1021/acsomega.4c00301
ACS Omega 2024, 9, 21006−21015

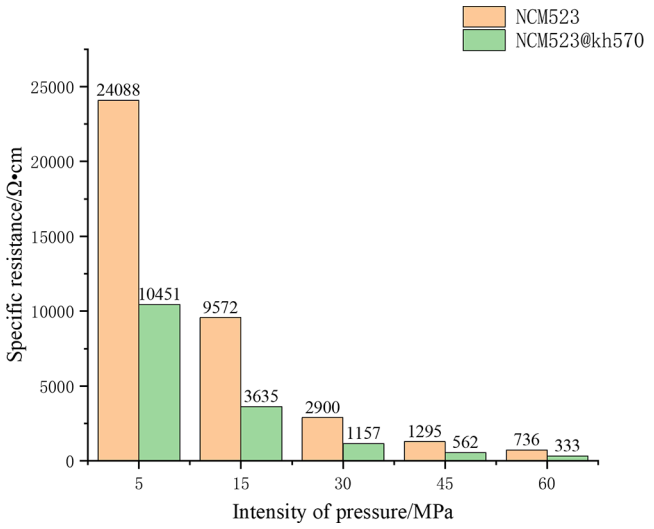

Figure 5. Specific resistance of electrodes under different levels of pressure intensity.

kh570 samples represented by the black and blue curves, respectively. The first and second cycles of the CV curves (2.8−4.3 V) are shown in Figure 6a,b, respectively. The NCM523 and NCM523@kh570 batteries both exhibit a pair of redox peaks, which are associated with the H1 (hexagonal 1) to M (monoclinic) phase transition.[34] In the first cycle, the cathodic peaks for NCM523 and NCM523@kh570 batteries are >4.3 (due to significant polarization of the battery, only the left half of the cathodic peak can be observed) and 3.967 V, respectively. Their anodic peak potentials are 3.579 and 3.683 V, respectively. The potential interval (ΔV) between the cathodic and anodic peaks of NCM523@kh570 electrodes is relatively narrower than that observed for NCM523 electrodes, suggesting reduced polarization in NCM523@kh570 electrodes. The same results were obtained in the second through fifth cycle voltammetry curves, as shown in Figures 6b and S3a−c. The NiO, Li_2CO_3, and LiOH easily formed on the cathode surface during the aqueous electrodes process are electrochemically inert and can increase impedance and polarization of batteires.[16,32] The resistance of electrodes also has a significant impact on polarization of batteries. The lower polarization observed in NCM523@kh570 electrodes can be attributed to the presence of the hydrophobic layers, which effectively reduces direct contact between the cathode particles and water during the aqueous process, thereby surppressing future Li^+/H^+ cation exchange reactions, reducing the specific resistance of electrodes and reducing the occurrence of microcracks. Compared to the first CV cycle, both NCM523 and NCM523@kh570 electrodes exhibit a significant reduction in the cathodic peak during the second CV cycle. This reduction is attributed to the formation of a solid electrolyte (CEI film) in the initial cycle.[35]

The specific capacity at different current rates is shown in Figure 6c. The specific capacities of the NCM523 and NCM523@kh570 electrodes are 163.23 mA h g^{-1} and 160.8092 mA h g^{-1} at 0.1C, respectively. They are similar. However, when the current rate increases to 0.5−5C, the NCM523@kh570 electrodes exhibit superior specific capacity performance compared to the NCM523 electrodes. This contributes to the reduction in polarization of NCM523@kh570 electrodes. The first charge−discharge curves are shown in Figure 6d. The NCM523@kh570 electrodes exhibit a lower charge voltage plateau and a higher discharge plateau in

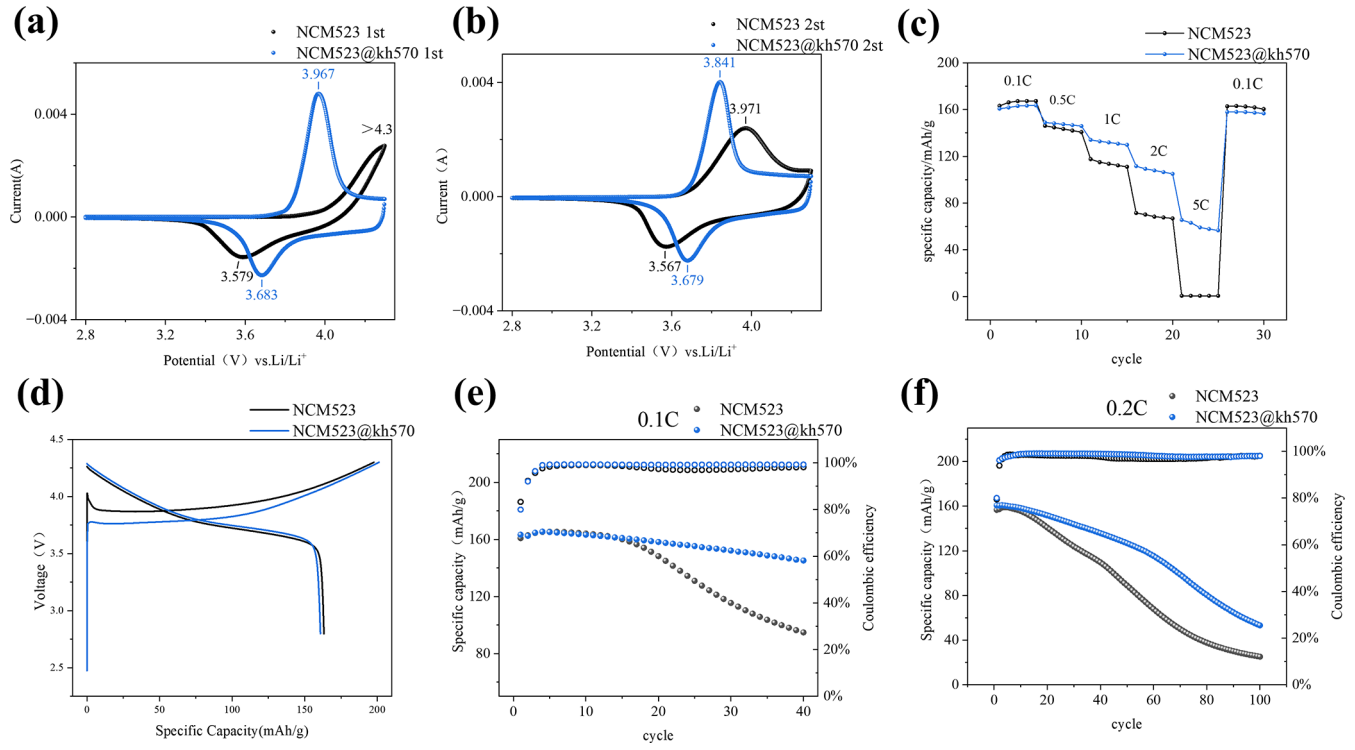

Figure 6. Voltammetry curves of NCM523 and NCM523@kh570 batteries at (a) the first cycle and (b) the second cycle; (c) the specific capacity of NCM523 and NCM523@kh570 batteries at different current rates; and (d) the first charge−discharge curve at 0.1C; the cycle curves at (e) 0.1C and (f) 0.2C.

https://doi.org/10.1021/acsomega.4c00301
ACS Omega 2024, 9, 21006−21015

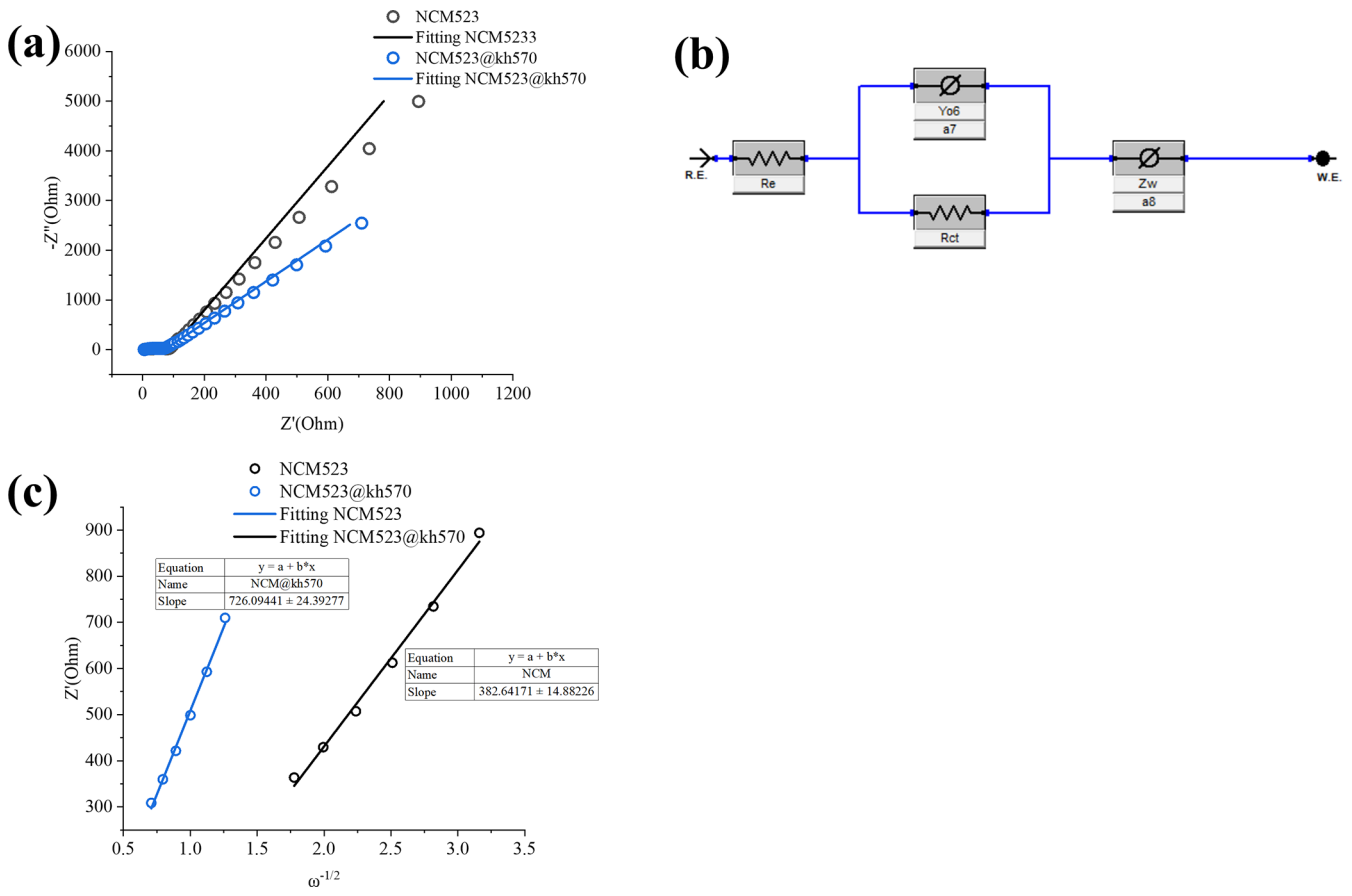

Figure 7. (a) Nyquist plot of the NCM523 and NCM523@kh570 batteries. (b) Equivalent circuit model of EIS spectra. (c) Graph of $Z'-\omega^{-1/2}$.

comparison to those of the NCM523 electrodes, thereby providing further evidence of the reduced polarization characteristics.

The cycling curves of the batteries are presented in Figure 6e,f. The specific capacity values of NCM523 and NCM523@kh570 electrodes after 40 cycles at 0.1C are 94.78 and 145 mA h g^{-1}, respectively. After 100 cycles at 0.2C, the specific capacity values of NCM523 and NCM523@kh570 electrodes are 25.22 and 53 mA h g^{-1}, respectively. The data demonstrate that the NCM523@kh570 electrodes exhibit superior cycle performance. The existence of microcracks inside the cathode is an important factor in reducing the cycling perform of polycrystalline cathode $LiNi_xCo_yMn_{1-x-y}O_2$.[36] During cycling, the occurrence of microcracks leads to the formation of additional reaction sites with electrolytes, resulting in the generation of novel solid electrolyte interfaces (CEI) that can consume more electrolytes and increase the impedance. The corrosion of the Al current collector also impacts the cyclic performance. As previously mentioned, the NCM523@kh570 particles were encapsulated with hydrophobic layers to mitigate microcrack formation and reduce the corrosion of the Al current collector. Consequently, the NCM523@kh570 electrodes exhibited an improved cycling stability.

Figure 7a shows the electrochemical impedance (EIS) curves of the NCM523 and NCM523@kh570 batteries, and Figure 7b shows their equivalent circuit model. The intersection of the semicircle with the x-axis at high frequency is related to Ohmic resistance (R_e). A semicircular shape is observed at intermediate frequencies, which reflects the charge transfer resistance (R_{ct}). At low frequencies, it appears as a slash, which is related to Warburg resistance (Z_W). The data obtained from fitting the equivalent circuit are presented in Table 1. Compared to NMC523 electrodes, the R_{ct} of the

Table 1. Simulation Data of EIS

cathodes	R_e (Ω)	R_{ct} (Ω)
NCM523	1.619	88.93
NCM523@kh570	4.952	67.36

NMC523@kh570 electrodes is lower. This can be attributed to the presence of hydrophobic coating layers, which suppresses the Li^+/H^+ reaction between cathode particles and water by minimizing direct contact. It is noted that the R_e of NCM523@kh570 batteries is increased slightly due to the nonelectronic conductive of the coating layer. The Warburg slope can be observed in the low-frequency region. The real part of the current corresponds to the Warburg factor σ as described by equation[37] (4)

$$Z' = R_e + R_{ct} + \sigma\omega^{-1/2} \quad (4)$$

The diffusion coefficient of Li^+ is inversely related to that of σ^2. To further investigate the diffusion behavior of Li^+ in the electrodes, we investigated the low-frequency region where the dominant diffusion mechanism occurs. A plot of Z' against angular frequency $\omega^{-1/2}$ is shown in Figure 7c. The results demonstrate that the NCM523@kh570 electrodes exhibit a steeper slope, suggesting lower Li^+ diffusion coefficients. This observation can be attributed to the nonionic conductivity of

https://doi.org/10.1021/acsomega.4c00301
ACS Omega 2024, 9, 21006−21015

the hydrophobic polymer coating layer, which reduces the diffusion of Li^+ within the electrodes.

4. CONCLUSIONS

In conclusion, we utilized kh570 to generate an organic amorphous coating layer with a thickness of 2−3 nm on the surface of the $LiNi_{0.5}Co_{0.2}Mn_{0.3}O_2$ cathode. It transforms the surface properties of the cathode particles from hydrophilic to hydrophobic due to the presence of numerous hydrophobic ester bonds in the coating layers. Although the Ohmic resistance (R_e) of the NCM523@kh570 electrodes slightly increases due to the no-electrically conductive and the diffusion of Li^+ slightly decreases due to the no-ion conductive nature of the coating layer, it effectively mitigates direct contact between cathode particles and water, and reducing formation of microcracks within cathode particles during aqueous electrode processing and subsequently suppressing Li^+/H^+ cation exchange reactions. Compared to the NCM523 aqueous electrodes, the NCM523@kh570 aqueous electrodes exhibit smaller charge transfer resistance (R_{ct}), lower polarization, higher current rate performance, and superior cycling performance. This coating strategy is applicable not only to the $LiNi_{0.5}Co_{0.2}Mn_{0.3}O_2$ cathode but also to other cathode materials in aqueous electrodes processing.

■ ASSOCIATED CONTENT

Supporting Information

The Supporting Information is available free of charge at https://pubs.acs.org/doi/10.1021/acsomega.4c00301.

Contact angle between cathode power and water, the multifunctional resistance testing instrument and CV curves of third, fourth, and fifth cycles (PDF)

■ AUTHOR INFORMATION

Corresponding Author

Chun Huang − *Shanghai Advanced Research Institute, Chinese Academy of Sciences, Shanghai 201210, China*; Email: annhuang2018@gmail.com

Authors

Wenchang Jiang − *Shanghai Advanced Research Institute, Chinese Academy of Sciences, Shanghai 201210, China; University of the Chinese Academy of Sciences, Beijing 100049, China*; orcid.org/0009-0004-9305-7483

Yilan Jiang − *Institute of Corrosion Science and Technology, Guangzhou 510530, China*

Complete contact information is available at: https://pubs.acs.org/10.1021/acsomega.4c00301

Author Contributions

Wenchang Jiang conducted all experiments, analyzed the data, and wrote the manuscript; Yilan Jiang contributed to obtaining SEM images; and Chun Huang supervised the project and reviewed the manuscript.

Notes

The authors declare no competing financial interest.

■ ACKNOWLEDGMENTS

This work was supported by Shanghai Zhangjiang National Independent Innovation Demonstration Zone Special Development Fund Major Project (phase II).

■ REFERENCES

(1) Li, M.; Lu, J.; Chen, Z.; Amine, K. 30 Years of Lithium-Ion Batteries. *Adv. Mater.* **2018**, *30*, No. e180056130.

(2) *Lithium-ion Battery Market Size, Share & Trends Analysis Report by Product (LCO, LFP, NCA, LMO, LTO, NMC), by Application (Consumer Electronics, Energy Storage Systems, Industrial), by Region, and Segment Forecasts, 2022−2030*; Research and Markets.

(3) Solef Corp. Solef® PVDF for Li-Ion Batteries, 2023. https://www.solvay.com/en/brands/solef-pvdf/li-ion-batteries (accessed November 1, 2023).

(4) (a) Bauer, W.; Nötzel, D. Rheological properties and stability of NMP based cathode slurries for lithium ion batteries. *Ceram. Int.* **2014**, *40* (3), 4591−4598. (b) Sung, S. H.; Kim, S.; Park, J. H.; Park, J. D.; Ahn, K. H. Role of PVDF in Rheology and Microstructure of NCM Cathode Slurries for Lithium-Ion Battery. *Mater.* **2020**, *13* (20), 4544.

(5) (a) Sitarek, K.; Stetkiewicz, J. Assessment of reproductive toxicity and gonadotoxic potential of N-methyl-2-pyrrolidone in male rats. *Int. J. Occup. Med. Environ. Health* **2008**, *21* (1), 73−80. (b) Lee, K. P.; Chromey, N. C.; Culik, R.; Barnes, J. R.; Schneider, P. W. Toxicity of N-methyl-2-pyrrolidone (NMP): teratogenic, subchronic, and two-year inhalation studies. *Fundam. Appl. Toxicol.* **1987**, *9* (2), 222−235.

(6) (a) Li, J.; Fleetwood, J.; Hawley, W. B.; Kays, W. From Materials to Cell: State-of-the-Art and Prospective Technologies for Lithium-Ion Battery Electrode Processing. *Chem. Rev.* **2022**, *122* (1), 903−956. (b) Buqa, H.; Holzapfel, M.; Krumeich, F.; Veit, C.; Novák, P. Study of styrene butadiene rubber and sodium methyl cellulose as binder for negative electrodes in lithium-ion batteries. *J. Power Sources* **2006**, *161* (1), 617−622.

(7) Kuenzel, M.; Choi, H.; Wu, F.; Kazzazi, A.; Axmann, P.; Wohlfahrt-Mehrens, M.; Bresser, D.; Passerini, S. Co-Crosslinked Water-Soluble Biopolymers as a Binder for High-Voltage $LiNi_{0.5}Mn_{1.5}O^4$ |Graphite Lithium-Ion Full Cells. *ChemSusChem* **2020**, *13* (10), 2650−2660.

(8) Sun, M.; Zhong, H.; Jiao, S.; Shao, H.; Zhang, L. Investigation on Carboxymethyl Chitosan as New Water Soluble Binder for $LiFePO_4$ Cathode in Li-Ion Batteries. *Electrochim. Acta* **2014**, *127*, 239−244.

(9) Zhang, G.; Qiu, B.; Xia, Y.; Wang, X.; Gu, Q.; Jiang, Y.; He, Z.; Liu, Z. Double-helix-superstructure aqueous binder to boost excellent electrochemical performance in Li-rich layered oxide cathode. *J. Power Sources* **2019**, *420*, 29−37.

(10) Loeffler, N.; Kopel, T.; Kim, G.-T.; Passerini, S. Polyurethane Binder for Aqueous Processing of Li-Ion Battery Electrodes. *J. Electrochem. Soc.* **2015**, *162* (14), A2692−A2698.

(11) Prasanna, K.; Subburaj, T.; Jo, Y. N.; Lee, W. J.; Lee, C. W. Environment-friendly cathodes using biopolymer chitosan with enhanced electrochemical behavior for use in lithium ion batteries. *ACS Appl. Mater. Interfaces* **2015**, *7* (15), 7884−7890.

(12) (a) Zhao, T.; Chang, L.; Ji, R.; Chen, S.; Jin, X.; Zheng, Y.; Huang, X.; Shen, J.; Zhang, Y. Construction of high-performance Li-rich Mn-based cathodes assisted by a novel water-soluble LiPAA binder. *J. Mater. Sci.: Mater. Electron.* **2022**, *33* (20), 16383−16395. (b) Su, A.; Pang, Q.; Chen, X.; Dong, J.; Zhao, Y.; Lian, R.; Zhang, D.; Liu, B.; Chen, G.; Wei, Y. Lithium poly-acrylic acid as a fast Li^+ transport media and a highly stable aqueous binder for $Li_3V_2(PO_4)_3$ cathode electrodes. *J. Mater. Chem. A* **2018**, *6* (46), 23357−23365.

(13) (a) Ibing, L.; Gallasch, T.; Schneider, P.; Niehoff, P.; Hintennach, A.; Winter, M.; Schappacher, F. M. Towards water based ultra-thick Li ion battery electrodes - A binder approach. *J. Power Sources* **2019**, *423*, 183−191. (b) Wang, Z.; Dupré, N.; Gaillot, A.-C.; Lestriez, B.; Martin, J.-F.; Daniel, L.; Patoux, S.; Guyomard, D. CMC as a binder in $LiNi_{0.4}Mn_{1.6}O_4$ 5V cathodes and their electrochemical performance for Li-ion batteries. *Electrochim. Acta* **2012**, *62*, 77−83.

(14) Ma, Y.; Ma, J.; Cui, G. Small things make big deal: Powerful binders of lithium batteries and post-lithium batteries. *Energy Storage Mater.* **2019**, *20*, 146−175.

(15) (a) Li, C.-C.; Lee, J.-T.; Lo, C.-Y.; Wu, M.-S. Effects of PAA-NH_4 Addition on the Dispersion Property of Aqueous $LiCoO_2$ Slurries and the Cell Performance of As-Prepared $LiCoO_2$ Cathodes. *Electrochem. Solid-State Lett.* **2005**, *8*, A509. (b) Li, C.-C.; Lee, J.-T.; Peng, X.-W. Improvements of Dispersion Homogeneity and Cell Performance of Aqueous-Processed $LiCoO_2$ Cathodes by Using Dispersant of PAA - NH_4. *J. Electrochem. Soc.* **2006**, *153*, A809. (c) Zhong, H.; Sun, M.; Li, Y.; He, J.; Yang, J.; Zhang, L. The polyacrylic latex: an efficient water-soluble binder for Li-$Ni_{1/3}Co_{1/3}Mn_{1/3}O_2$ cathode in Li-ion batteries. *J. Solid State Electrochem.* **2016**, *20* (1), 1−8. (d) Karuppiah, S.; Franger, S.; Nallathamby, K. Water-Soluble Green Binder for $Li_4Ti_5O_{12}$ Anodes: Effect of Binder Choice on Lithium Storage. *ChemElectroChem* **2018**, *5* (2), 343−349.

(16) Shkrob, I. A.; Gilbert, J. A.; Phillips, P. J.; Klie, R.; Haasch, R. T.; Bareño, J.; Abraham, D. P. Chemical Weathering of Layered Ni-Rich Oxide Electrode Materials: Evidence for Cation Exchange. *J. Electrochem. Soc.* **2017**, *164* (7), A1489−A1498.

(17) Liu, H.; Yang, Y.; Zhang, J. Reaction mechanism and kinetics of lithium ion battery cathode material $LiNiO_2$ with CO_2. *J. Power Sources* **2007**, *173* (1), 556−561.

(18) Hartmann, L.; Pritzl, D.; Beyer, H.; Gasteiger, H. A. Evidence for Li^+/H^+ Exchange during Ambient Storage of Ni-Rich Cathode Active Materials. *J. Electrochem. Soc.* **2021**, *168* (7), 070507.

(19) (a) Doberdò, I.; Löffler, N.; Laszczynski, N.; Cericola, D.; Penazzi, N.; Bodoardo, S.; Kim, G.-T.; Passerini, S. Enabling aqueous binders for lithium battery cathodes - Carbon coating of aluminum current collector. *J. Power Sources* **2014**, *248*, 1000−1006. (b) Sahore, R.; Wood, D. L.; Kukay, A.; Grady, K. M.; Li, J.; Belharouak, I. Towards Understanding of Cracking during Drying of Thick Aqueous-Processed $LiNi_{0.8}Mn_{0.1}Co_{0.1}O_2$ Cathodes. *ACS Sustainable Chem. Eng.* **2020**, *8* (8), 3162−3169. (c) Ibing, L.; Gallasch, T.; Friesen, A.; Niehoff, P.; Hintennach, A.; Winter, M.; Börner, M. The role of the pH value in water-based pastes on the processing and performance of Ni-rich $LiNi_{0.5}Mn_{0.3}Co_{0.2}O_2$ based positive electrodes. *J. Power Sources* **2020**, *475*, 228608. (d) Wood, M.; Li, J.; Ruther, R. E.; Du, Z.; Self, E. C.; Meyer, H. M.; Daniel, C.; Belharouak, I.; Wood, D. L. Chemical stability and long-term cell performance of low-cobalt, Ni-Rich cathodes prepared by aqueous processing for high-energy Li-Ion batteries. *Energy Storage Mater.* **2020**, *24*, 188−197. (e) Church, B. C.; Kaminski, D. T.; Jiang, J. Corrosion of aluminum electrodes in aqueous slurries for lithium-ion batteries. *J. Mater. Sci.* **2014**, *49* (8), 3234−3241.

(20) Hofmann, M.; Kapuschinski, M.; Guntow, U.; Giffin, G. A. Implications of Aqueous Processing for High Energy Density Cathode Materials: Part I. Ni-Rich Layered Oxides. *J. Electrochem. Soc.* **2020**, *167* (14), 140512.

(21) Pillai, A. M.; Salini, P. S.; John, B.; Devassy, M. T. Aqueous Binders for Cathodes: A Lodestar for Greener Lithium Ion Cells. *Energy Fuels* **2022**, *36* (10), 5063−5087.

(22) (a) Bichon, M.; Sotta, D.; Dupre, N.; De Vito, E.; Boulineau, A.; Porcher, W.; Lestriez, B. Study of Immersion of Li-$Ni_{0.5}Mn_{0.3}Co_{0.2}O_2$ Material in Water for Aqueous Processing of Positive Electrode for Li-Ion Batteries. *ACS Appl. Mater. Interfaces* **2019**, *11* (20), 18331−18341. (b) Toma, T.; Maezono, R.; Hongo, K. Electrochemical Properties and Crystal Structure of Li^+/H^+ Cation-Exchanged $LiNiO_2$. *ACS Appl. Energy Mater.* **2020**, *3* (4), 4078−4087.

(23) Tanabe, T.; Gunji, T.; Honma, Y.; Miyamoto, K.; Tsuda, T.; Mochizuki, Y.; Kaneko, S.; Ugawa, S.; Lee, H.; Ohsaka, T.; et al. Preparation of Water-Resistant Surface Coated High-Voltage $LiNi_{0.5}Mn_{1.5}O_4$ Cathode and Its Cathode Performance to Apply a Water-Based Hybrid Polymer Binder to Li-Ion Batteries. *Electrochim. Acta* **2017**, *224*, 429−438.

(24) Tanabe, T.; Liu, Y.; Miyamoto, K.; Irii, Y.; Maki, F.; Gunji, T.; Kaneko, S.; Ugawa, S.; Lee, H.; Ohsaka, T.; et al. Synthesis of water-resistant thin TiO_x layer-coated high-voltage and high-capacity $LiNi_aCo_bAl_{1-a-b}O_2$ ($a > 0.85$) cathode and its cathode performance to apply a water-based hybrid polymer binder to Li-Ion batteries. *Electrochim. Acta* **2017**, *258*, 1348−1355.

(25) (a) Hofmann, M.; Nagler, F.; Guntow, U.; Sextl, G.; Giffin, G. A. Long-Term Cycling Performance of Aqueous Processed Ni-Rich $LiNi_{0.8}Co_{0.15}Al_{0.05}O_2$ Cathodes. *J. Electrochem. Soc.* **2021**, *168* (6), 060511. (b) Hofmann, M.; Nagler, F.; Kapuschinski, M.; Guntow, U.; Giffin, G. A. Surface Modification of $LiNi_{0.8}Co_{0.15}Al_{0.05}$ O_2 Particles via Li_3 PO_4 Coating to Enable Aqueous Electrode Processing. *ChemSusChem* **2020**, *13* (22), 5962−5971.

(26) Watanabe, T.; Yokokawa, T.; Yamada, M.; Kurosumi, S.; Ugawa, S.; Lee, H.; Irii, Y.; Maki, F.; Gunji, T.; Wu, J.; et al. Surface coating of a $LiNi_xCo_yAl_{1-x-y}O_2$($x > 0.85$) cathode with $Li_3PO_4$for applying a water-based hybrid polymer binder during Li-ion battery preparation. *RSC Adv.* **2021**, *11* (59), 37150−37161.

(27) (a) Zhang, M.; Zhu, H.; Xi, B.; Tian, Y.; Sun, X.; Zhang, H.; Wu, B. Surface Hydrophobic Modification of Biochar by Silane Coupling Agent KH-570. *Processes* **2022**, *10* (2), 301. (b) Wang, Z.; Yuan, L.; Liang, G.; Gu, A. Mechanically durable and self-healing super-hydrophobic coating with hierarchically structured KH570 modified SiO_2-decorated aligned carbon nanotube bundles. *Chem. Eng. J.* **2021**, *408*, 127263. (c) Kunst, S. R.; Ludwig, G. A.; Cardoso, H. R. P.; Santana, J. A.; Sarmento, V. H. V.; Malfatti, C. d. F. Hybrid films with (trimethoxysilylpropyl) methacrylate (TMSM), poly (methyl methacrylate) PMMA and tetraethoxysilane (TEOS) applied on tinplate. *Mater. Res.* **2014**, *17* (suppl 1), 75−81.

(28) Li, Y.; Wang, Z.-T.; Liu, G.; Wang, J.; Wang, J. Boosting the electrochemical performance of $LiNi_{0.8}Co_{0.1}Mn_{0.1}O_2$ cathode materials with $Zn_3(PO_4)_2$ surface coating. *Adv. Powder Technol.* **2021**, *32* (12), 4651−4657.

(29) Yu, H.; Wang, S.; Hu, Y.; He, G.; Bao, L. Q.; Parkin, I. P.; Jiang, H. Lithium-conductive $LiNbO_3$ coated high-voltage Li-$Ni_{0.5}Co_{0.2}Mn_{0.3}O_2$ cathode with enhanced rate and cyclability. *Green Energy Environ.* **2022**, *7* (2), 266−274.

(30) Bauer, W.; Nötzel, D.; Wenzel, V.; Nirschl, H. Influence of dry mixing and distribution of conductive additives in cathodes for lithium ion batteries. *J. Power Sources* **2015**, *288*, 359−367.

(31) Azhari, L.; Zhou, X.; Sousa, B.; Yang, Z.; Gao, G.; Wang, Y. Effects of Extended Aqueous Processing on Structure, Chemistry, and Performance of Polycrystalline $LiNi_xMn_yCo_zO_2$ Cathode Powders. *ACS Appl. Mater. Interfaces* **2020**, *12* (52), 57963−57974.

(32) (a) Lee, W.; Lee, S.; Lee, E.; Choi, M.; Thangavel, R.; Lee, Y.; Yoon, W.-S. Destabilization of the surface structure of Ni-rich layered materials by water-washing process. *Energy Storage Mater.* **2022**, *44*, 441−451. (b) Wu, F.; Dong, J.; Chen, L.; Chen, G.; Shi, Q.; Nie, Y.; Lu, Y.; Bao, L.; Li, N.; Song, T.; et al. Removing the Intrinsic NiO Phase and Residual Lithium for High-Performance Nickel-Rich Materials. *Energy Mater. Adv.* **2023**, *4*, 0007.

(33) Peng, C.; Liu, F.; Wang, Z.; Wilson, B. P.; Lundström, M. Selective extraction of lithium (Li) and preparation of battery grade lithium carbonate (Li_2CO_3) from spent Li-ion batteries in nitrate system. *J. Power Sources* **2019**, *415*, 179−188.

(34) Fang, J.; Ding, Z.; Ling, Y.; Li, J.; Zhuge, X.; Luo, Z.; Ren, Y.; Luo, K. Green recycling and regeneration of $LiNi_{0.5}Co_{0.2}Mn_{0.3}O_2$ from spent Lithium-ion batteries assisted by sodium sulfate electrolysis. *Chem. Eng. J.* **2022**, *440*, 135880.

(35) Ryu, H. H.; Park, G. T.; Yoon, C. S.; Sun, Y. K. Microstructural Degradation of Ni-Rich $Li[Ni_xCo_yMn_{1-x-y}]O_2$ Cathodes During Accelerated Calendar Aging. *Small* **2018**, *14* (45), No. e1803179.

(36) (a) Park, G.-T.; Park, N.-Y.; Noh, T.-C.; Namkoong, B.; Ryu, H.-H.; Shin, J.-Y.; Beierling, T.; Yoon, C. S.; Sun, Y.-K. High-performance Ni-rich $Li[Ni_{0.9-x}Co_{0.1}Al_x]O_2$ cathodes *via* multi-stage microstructural tailoring from hydroxide precursor to the lithiated oxide. *Energy Environ. Sci.* **2021**, *14* (9), 5084−5095. (b) Ryu, H.-H.; Park, K.-J.; Yoon, C. S.; Sun, Y.-K. Capacity Fading of Ni-Rich $Li[Ni_xCo_yMn_{1-x-y}]O_2$ ($0.6 \leq x \leq 0.95$) Cathodes for High-Energy-Density Lithium-Ion Batteries: Bulk or Surface Degradation? *Chem. Mater.* **2018**, *30* (3), 1155−1163. (c) Li, J.; Zhou, Z.; Luo, Z.; He, Z.; Zheng, J.; Li, Y.; Mao, J.; Dai, K. Microcrack generation and modification of Ni-rich cathodes for Li-ion batteries: A review. *Sustainable Mater. Technol.* **2021**, *29*, No. e00305. (d) Liao, Q.-T.; Guo, S.-J.; Qi, M.-Y.; Zhang, S.-D.; Ma, P.-Z.; Li, J.-Y.; Cao, A.-M.;

https://doi.org/10.1021/acsomega.4c00301
ACS Omega 2024, 9, 21006−21015

Wan, L.-J. The genesis and control of microcracks in nickel-rich cathode materials for lithium-ion batteries. *Sustainable Energy Fuels* **2023**, 7 (19), 4805−4824. (e) Liu, X.; Zhan, X.; Hood, Z. D.; Li, W.; Leonard, D. N.; Manthiram, A.; Chi, M. Essential effect of the electrolyte on the mechanical and chemical degradation of $LiNi_{0.8}Co_{0.15}Al_{0.05}O_2$ cathodes upon long-term cycling. *J. Mater. Chem. A* **2021**, *9* (4), 2111−2119.

(37) Lee, Y.-G.; Lee, J.; An, G. H. Free-standing manganese oxide on flexible graphene films as advanced electrodes for stable, high energy-density solid-state zinc-ion batteries. *Chem. Eng. J.* **2021**, *414*, 128916.

https://doi.org/10.1021/acsomega.4c00301
ACS Omega 2024, 9, 21006−21015